AIAA JOURNAL
Vol. 35, No. 12, December 1997

Prediction of Active Control of Subsonic Centrifugal Compressor Rotating Stall

P. B. Lawless* and S. Fleeter†
Purdue University, West Lafayette, Indiana 47907

A mathematical model is developed to predict the suppression of rotating stall in a centrifugal compressor with a vaned diffuser. This model is based on the employment of a control vortical waveform generated upstream of the impeller inlet to damp weak potential disturbances that are the early stages of rotating stall. The control system is analyzed by matching the perturbation pressure in the compressor inlet and exit flowfields with a model for the unsteady behavior of the compressor. The model was effective at predicting the stalling behavior of the Purdue Low-Speed Centrifugal Compressor for two distinctly different stall patterns. Predictions made for the effect of a controlled inlet vorticity wave on the stability of the compressor show that, for minimum control wave magnitudes, on the order of the total inlet disturbance magnitude, significant damping of the instability can be achieved. For control wave amplitudes of sufficient amplitude, the control phase angle appears to be the most important factor in maintaining a stable condition in the compressor.

Nomenclature

a	= acoustic speed
a_0	= dimensionless acoustic speed ($\bar{a}/U$)
B_n, C_n	= complex constants
D	= diffusion factor
$\tilde{\mathbf{D}}$	= linearized substantial derivative
i	= $\sqrt{-1}$
$\boldsymbol{i}$	= unit vector, relative frame
$\boldsymbol{j}$	= unit vector, absolute frame
k	= reduced propagation frequency
L	= propagation parameter; Eq. (32)
M	= Mach number
n	= spatial wave number
p	= pressure
q	= dynamic pressure
R	= mean inlet radius
s	= flow path distance, absolute frame
s^*	= flow path distance, relative frame
t	= time
U	= wheel speed at mean inlet radius
V	= absolute velocity
W	= relative velocity
w	= specific work
Z	= complex control gain
z	= axial coordinate
α	= direction cosine
γ	= specific heat ratio
η_c	= isentropic efficiency
θ	= tangential coordinate
κ, λ	= separation constant
ξ	= phase lag angle
ρ	= density
Φ	= disturbance velocity potential
ϕ	= inlet flow coefficient
ψ	= pressure rise coefficient
ω	= frequency

Subscripts and Superscripts

asy	= asymmetric
D	= diffuser
e	= exit
I	= impeller
i	= inlet
m	= mean path
p	= potential component
t	= total property
u	= unsteady
v	= vortical component
$\bar{X}$	= time mean value
X'	= perturbation value
$*$	= impeller relative

Received May 7, 1996; revision received Aug. 22, 1997; accepted for publication Sept. 1, 1997.

*Assistant Professor, School of Mechanical Engineering. Member AIAA.
†McAllister Distinguished Professor, School of Mechanical Engineering. Associate Fellow AIAA.

Introduction

THE operating range of a turbomachinery compressor is bounded by the surge and choke lines on the system performance map. The barrier posed by the surge line is of particular interest due to its proximity to the maximum efficiency point of the compressor. Current practice in turbomachinery design is to plan the operating points for the machine in a region far enough removed from the surge line so as to prevent the onset of instability.

The surge line separates the regions of stable and unstable compressor operation. The term surge line is somewhat misleading because surge is only one of the possible phenomena that result when this boundary is reached. In general, the types of instabilities found in turbomachines can be categorized as surge or rotating stall. Surge takes the form of a global, circumferentially symmetric oscillation of the mass flow through the compression system. Surge is considered to be a phenomenon of the entire compression system, consisting of the compressor and the system into which it discharges. Rotating stall, in contrast, is an instability local to the compressor itself and is characterized by a circumferentially nonuniform mass deficit that propagates around the compressor annulus at a fraction of wheel speed.

There are numerous disadvantages for allowing a compressor to enter rotating stall. Not only is the performance of the compressor severely degraded in stall, but rotating stall may introduce dangerous unsteady aerodynamic excitation to impeller and diffuser vanes. For these reasons, attempts to increase the stable operating range of compressors have long been an area of vigorous research activity.

There are, at the minimum, two views of the triggering phenomena for a rotating stall condition in a compression system. The view of rotating stall as the growth and propagation of a finite separation zone has been supported by researchers such as Day,[1] who has observed such behavior in a low-speed axial compressor. Another theory on the evolution of rotating stall explains the phenomenon as the culmination of a process that begins with selective amplification of initially weak spatial harmonic waves in the compression system.

Investigations by McDougall et al.[2] and by Garnier et al.[3] provide evidence of such a rotating stall pathology in axial compressors. It appears that, for axial compressors, both mechanisms can play a role in the stall initiation process.

Rotating stall behavior for centrifugal compressors is less well understood than that for their axial counterparts. This is, in part, due to the variety of rotating stall conditions found in this type of compressor, with stall cell number, propagation speed, and growth rates observed to change with modifications in compressor geometry.[4] The possibility that the weak spatial waves seen as precursors to rotating stall in axial compressors may also play a role in the initiation of rotating stall in centrifugal machines has been suggested by analyses such as that of Moore,[5] which predicted the occurrence of waves of similar mode shape and wave speed as those observed in finite rotating stall patterns. More recently, experiments conducted by the present authors on a low-speed centrifugal compressor at Purdue University have shown that the stall process in that compressor is characterized by an initially weak, spatially coherent disturbance that develops over a finite period of time into a rotating stall condition.[6]

Because of the promise of achieving increased stall margin, active stall control schemes have recently become an area of increased research activity. An analysis by Epstein et al.[7] investigated the concept that an axial compression system could have its operating range extended by the introduction of a controlled inlet distortion, which would damp the weak precursors of a rotating stall condition. Such a system has since been demonstrated to be an effective range extension technique on a low-speed axial compressor by Paduano et al.[8]

An earlier work by the present authors[9] concerned the development of a mathematical model to investigate the effectiveness of a control system for a centrifugal compressor similar in operation to that proposed by Epstein et al.[7] and demonstrated by Paduano et al.[8] for an axial compressor. In that model, the effectiveness of a phased vorticity wave introduced into the inlet of a centrifugal compressor in extending the stable operating range was investigated.[9] A basic assumption in that analysis was that, in its early stages, rotating stall is well represented as a weak disturbance that grows in a region of preferential amplification on the performance map into a finite stall condition.

This paper is directed at extending the model of Ref. 9 to allow the relaxation of two key assumptions made in the analysis. The first, that of incompressible flow, is replaced by a less restrictive assumption of subsonic compressible flow in the current model. The second related assumption made in the initial analysis was that of infinite propagation speed for the control waveform. The current effort is directed at allowing for finite propagation speed through the compressor and determining the result such a spatial time lag will have on the effectiveness of the control.

In addition, the model is applied to a low-speed centrifugal compressor with a radial vaned diffuser to predict the stall point. The results of this analysis are compared with spatial domain stall initiation data recently taken in an experimental investigation of rotating stall initiation in this facility.

Mathematical Model

Centrifugal Compressor

A sketch of the assumed centrifugal compressor geometry is given in Fig. 1. This geometry is based on the Purdue Low-Speed Centrifugal Compressor Facility at Purdue University. Air is taken in axially through the inlet at position 1 and flows along the duct past an array of vorticity generators at position 2. The flow then enters the compressor rotor at position 3 ($z = 0$) and proceeds through the shrouded impeller, exiting into the vaneless space at position 4. From here the flow enters a series of vanes, exiting at an assumed constant flow angle and proceeding along a logarithmic spiral path to the exit plenum at position 5.

The pressure rise characteristic $\bar{\psi}(\bar{\phi})$ describes the behavior of the compressor under an axisymmetric velocity perturbation that enters in a quasisteady manner, as shown in Fig. 2. The portion of the curve up to the stall point represents a map of steady operating points that would be traversed by closing a downstream throttle. At flow rates below the stall point, the curve represents the pressure rise that would exist in the absence of any instability.

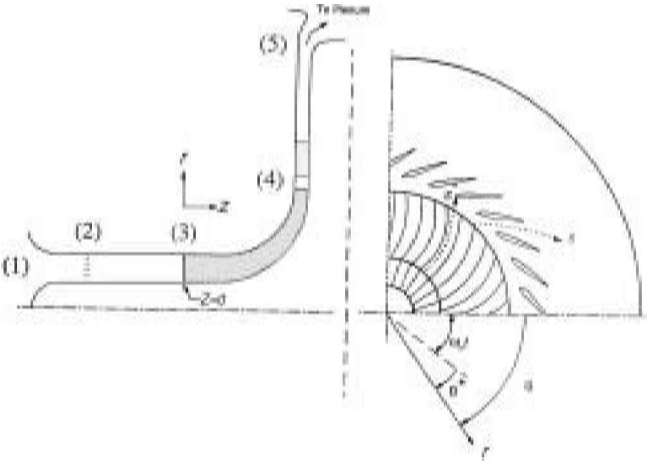

Fig. 1 Centrifugal compressor geometry.

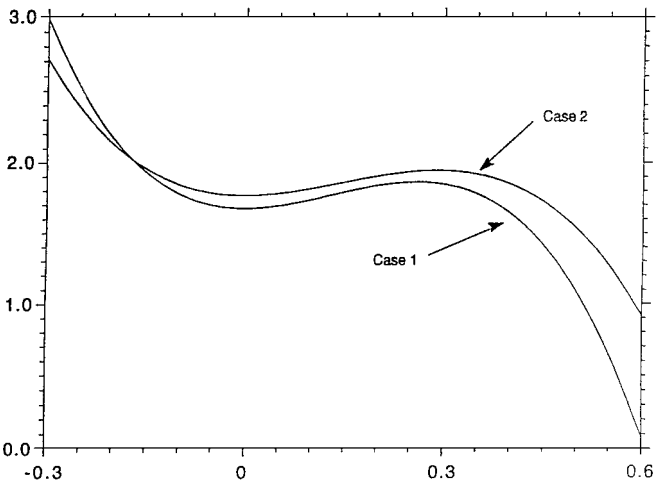

Fig. 2 Steady compressor pressure rise characteristic curves.

Inlet Flowfield

Upstream Potential Precursor

The flow in the intake annulus of the centrifugal compressor is assumed to be inviscid, two-dimensional, and subsonic. The unsteady flow is characterized by a small perturbation from the mean axial velocity of magnitude $\bar{V}$. The irrotational component of the flow in the inlet is described via a disturbance potential Φ, which decays to zero far upstream of the impeller inlet. The net inlet potential flow can then be represented as

$$\boldsymbol{V}(z, \theta, t) = \bar{V}\boldsymbol{i}_z + \nabla\Phi(z, \theta, t) \tag{1}$$

where $\Phi \to 0$ as $z \to -\infty$.

The linear wave equation that governs this flow is expressed as

$$\tilde{\mathbf{D}}^2\Phi = \bar{a}^2\nabla^2\Phi \tag{2}$$

where $\tilde{\mathbf{D}} = (\partial/\partial t) + \bar{V}\boldsymbol{i}_z \cdot \nabla$.

A solution to Eq. (2) after applying the far-field boundary conditions takes the form of

$$\Phi = \sum_{n=0}^{\infty} B_{n\pm} U \exp(\pm in\theta) \exp(\mp i\omega t) \exp[(|\lambda| \mp i\kappa\bar{M})^{z/R}] \tag{3}$$

where $B_{n\pm}$ are complex conjugate constants, n is the spatial mode, ω is the frequency, and λ and κ are separation constants that are related to the frequency and wave number as follows:

$$n = \sqrt{(1 - \bar{M}^2)(\kappa^2 + \lambda^2)}, \qquad \omega = \frac{\kappa\bar{a}(1 - \bar{M}^2)}{R} \tag{4}$$

In this linear model, superposition applies and each harmonic can be considered independently. In addition, by defining the perturbation values as deviations from the mean, the $n = 0$ contribution to

the summation is zero and is excluded from the following analysis. For convenience, the summation symbol will henceforth be dropped and the constant B_n will represent the complex amplitude of the first half of the conjugate pair of solutions that represent the contribution to Φ in Eq. (3).

The solution for the disturbance potential allows the axial and circumferential velocity perturbations in the irrotational inlet flow to be expressed as

$$V'_{zp} = (B_n U f/R)e^{i\omega t}e^{f(z/R)}e^{-in\theta}, \qquad V'_{\theta p} = -(in/f)V'_{zp} \quad (5)$$

where $f \equiv |\lambda| + i\kappa\bar{M}$ for convenience.

The function $f = f(\bar{M}, \lambda, \kappa)$ is now recast as a function of variables more suitable for the desired solution by noting the relationships of Eq. (4) and introducing the mean inlet flow coefficient $\bar{\phi} = \bar{V}/U$ and reduced frequency of propagation $k = \omega R/U$:

$$f(\bar{\phi}, n, k, a_0) = \frac{a_0\sqrt{n^2\left(a_0^2 - \bar{\phi}^2\right) - k^2} + ik\bar{\phi}}{a_0^2 - \bar{\phi}^2} \quad (6)$$

where $a_0 = \bar{a}/U$.

The static pressure perturbation in the inlet corresponding to the potential velocity perturbation is described by a linearized Bernoulli equation

$$p'_i = -\bar{\rho}_i\tilde{\mathbf{D}}\Phi \quad (7)$$

resulting in

$$p'_i = -\bar{\rho}_i V'_{zp}[(iR\omega/f) + \bar{V}] \quad (8)$$

Control Vortical Waveform

Upstream of the impeller inlet, the control waveform is generated from the array of vorticity generators. The nature of the vortical velocity perturbation is defined as simply convected and solenoidal and, thus, does not interact with the static pressure perturbation in the assumed two-dimensional flowfield of the inlet annulus.[10] This control velocity perturbation in the axial direction is assumed to be a fraction of the potential axial velocity perturbation at the compressor inlet face ($z = 0$). The form of this component can, therefore, be expressed as

$$V'_{zv} = (C_n U f/R)\exp(-in\theta)\exp\{i\omega[t - (z/\bar{V})]\} \quad (9)$$

where C_n is a complex constant and the subscript v denotes the vortical nature of the perturbation.

The preceding relationship and the requirement that the velocity perturbation be solenoidal results in the following expression for the circumferential velocity perturbation:

$$V'_{\theta v} = -(k/\bar{\phi}n)V'_{zv} \quad (10)$$

Total Pressure Perturbation

With the velocity and static pressure disturbances now defined for the inlet flowfield, the task of determining the inlet total pressure perturbation is undertaken. The expression for the total pressure of a perfect gas is

$$p_t = p\{1 + [(\gamma - 1)/2]\bar{M}^2\}^{(\gamma/\gamma - 1)} \quad (11)$$

The total and static pressures and Mach number are now separated into mean and perturbation quantities, and the binomial theorem is employed to arrive at an expression for the perturbation total pressure in the inlet:

$$\begin{aligned} p'_{ti} &= M'[\gamma\bar{p}\bar{M} + (\gamma/2)\bar{p}\bar{M}^3 + \cdots] \\ &\quad + p'[1 + (\gamma/2)\bar{M}^2 + (\gamma/8)\bar{M}^4 + \cdots] \\ &\quad + O(p'M') + O(M'^2) + \cdots \end{aligned} \quad (12)$$

The relationship between the perturbation Mach number and the perturbation velocity is expressed, under the assumption of constant total temperature in the inlet flow, as (see the Appendix)

$$M' = (V'/\bar{a})\left\{1 + [(\gamma - 1)/2]\left(\bar{\phi}^2/a_0^2\right)\right\} \quad (13)$$

Equation (13) is now used to transform Eq. (12) into a function of the mean flow coefficient, the perturbation pressure, and the perturbation velocity in the inlet as

$$p'_{ti} = (\bar{p}\gamma/\bar{a})G_1 V' + G_2 p'_i \quad (14)$$

where

$$G_1 \equiv \left\{1 + [(\gamma - 1)/2]\left(\bar{\phi}^2/a_0^2\right)\right\}\left[(\bar{\phi}/a_0) + \tfrac{1}{2}(\bar{\phi}/a_0)^3 + \cdots\right]$$

and

$$G_2 \equiv 1 + (\gamma/2)(\bar{\phi}/a_0)^2 + (\gamma/8)(\bar{\phi}/a_0)^4 + \cdots$$

As mentioned, the time-averaged flow in the inlet is axial. A mean path inlet velocity is now introduced such that

$$\boldsymbol{V}_{mi} = (\bar{V} + V'_{zi})\boldsymbol{j}_z + (V'_{\theta i})\boldsymbol{j}_\theta$$

giving the relations

$$\bar{V}_{mi} = \bar{V}_{zi}, \qquad V'_{mi} = V'_{zi} + O(V'V') \quad (15)$$

The expressions for potential and vortical velocity perturbations at the compressor inlet can now be expressed as perturbation inlet flow coefficients and be used to calculate the scaled total pressure perturbation:

$$p'_{ti}/\bar{\rho}U^2 = a_0 G_1\phi' - G_2[(ik/f) + \bar{\phi}](\phi' - \phi'_v) \quad (16)$$

where

$$\phi' = \left[\frac{V'_{zp} + V'_{zv}}{U}\right]_i, \qquad \phi'_v = \left[\frac{V'_{zv}}{U}\right]_i, \qquad \phi'_p\left[\frac{V'_{zp}}{U}\right]_i = \phi' - \phi'_v$$

Equation (16) is the required expression for the perturbation total pressure expressed in terms of inlet flow coefficient and reduced frequency of propagation.

Exit Boundary Condition

At the diffuser exit, the flow enters a large plenum scroll of constant static pressure at subsonic velocity. An abrupt expansion is assumed, resulting in the loss of all remaining dynamic pressure. The appropriate boundary condition at this point is an extinction condition on the static pressure perturbation,

$$p'_e = 0 \quad (17)$$

Unsteady Centrifugal Compressor Characteristic

The behavior of the centrifugal compressor under the influence of a small unsteady inlet flow distortion is modeled by introducing a correction to the mean flow pressure rise predicted by the compressor characteristic. This new, unsteady compressor characteristic curve takes the form

$$\psi = \bar{\psi} + \psi' = \frac{\bar{p}_e - \bar{p}_{ti}}{\bar{\rho}_i U^2} + \frac{p'_e - p'_{ti}}{\bar{\rho}_i U^2}$$

As a first step in developing an expression for the unsteady characteristic, ψ' is subdivided into the following terms:

$$\psi' = \psi'_{\Delta\bar{V}} + \left(1/\bar{\rho}_i U^2\right)(\Delta p'_{\Delta w} + \Delta p'_{u,\mathrm{asy},I} + \Delta p'_{u,\mathrm{asy},D}) \quad (18)$$

The first term of this expression represents the correction due to the axial velocity perturbation neglecting any unsteady, asymmetric effects and can be represented as an excursion along the steady characteristic curve. If the change in flow coefficient is small, the expression for the change in pressure coefficient is given by

$$\psi'_{\Delta\bar{V}} = \frac{\partial\bar{\psi}}{\partial\bar{\phi}}\phi' \quad (19)$$

The second term of Eq. (18) represents the pressure change due to a loss or gain of work done on the fluid because of the circumferential velocity perturbation in the inlet. This term is modeled as a small inlet prewhirl, taking the form

$$\Delta p'_{\Delta w} = \frac{\partial\Delta\bar{p}}{\partial\bar{w}}w'$$

where $w' = -V'_{\theta i}U$.

For a given mean flow isentropic efficiency $\bar{\eta}_c(\bar{\phi})$, the change in the mean flow static pressure across the compressor is given by

$$\bar{p} = \bar{p}_{ti}\left[\left(1 + \frac{\bar{\eta}_c \bar{w}}{C_p \bar{T}_{ti}}\right)^{(\gamma/\gamma-1)} - 1\right] - \Delta\bar{q} \tag{20}$$

Equations (5) and (10) give the total circumferential velocity perturbation at the impeller inlet, resulting in an expression for the perturbation work:

$$w' = U[(in/f)V'_{zp} + (k/\bar{\phi}n)V'_{zv}] \tag{21}$$

A diffusion factor $\bar{D}_D|_e$ is defined such that the dynamic pressure at the diffuser exit can be expressed in terms of the mean inlet velocity and a compressibility factor:

$$\bar{V}_e \equiv \bar{D}_D|_e \bar{V}, \qquad \bar{q}_e = F_c \bar{\rho}_e (\bar{D}_D|_e \bar{V})^2 \tag{22}$$

where the compressibility factor can be expressed as

$$F_c = \left[1 + \frac{1}{4}\left(\frac{\bar{D}_D|_e \bar{\phi}}{a_0|_e}\right)^2 + \frac{1}{40}\left(\frac{\bar{D}_D|_e \bar{\phi}}{a_0|_e}\right)^4 + \cdots\right]$$

After Eq. (20) is differentiated with respect to $\bar{w}$, Eqs. (21) and (22) are used to express the scaled pressure rise due to the work perturbation in terms of the mean and perturbation inlet flow coefficients:

$$\frac{\Delta p'_{\Delta w}}{\bar{\rho}_i U^2} = \bar{\eta}_c\left(\frac{in}{f}\phi'_p + \frac{k}{\bar{\phi}n}\phi'_v\right)\left[1 + \frac{1}{\bar{p}_{ti}}(\bar{q}_e + \bar{\rho}_i U^2 \bar{\psi})\right]^{1/\gamma} \tag{23}$$

The last two terms in Eq. (20) represent the pressure rise due to unsteady, asymmetric effects on the fluid in the impeller and diffuser, respectively. The basis for these corrections is that the unsteady, asymmetric pressure rise is balanced by the acceleration of fluid in the compressor. It is recognized that, even when operating with an axisymmetric flow in the inlet, the separated flow in the impeller and jet wake mixing in the vaneless space result in asymmetric flow in the compressor. It is suggested here, however, that distortion occurring in these regions would be on a scale of impeller blade or diffuser vane spacing, whereas the perturbations of interest are of circumferential scale. Hence, whereas the higher harmonic distortions may be generated, the essential character of the lower-order harmonic waves of interest here should be preserved. The pressure correction for the impeller is considered first, followed by that of the diffuser.

Impeller Correction

In a reference frame fixed to the impeller

$$\frac{1}{\rho}\nabla^* p_{u,\mathrm{asy},I} = \frac{W_\theta}{r}\frac{\partial \boldsymbol{W}}{\partial \theta^*} + \frac{\partial \boldsymbol{W}}{\partial t} \tag{24}$$

where $\boldsymbol{W}$ is the relative flow velocity and $\theta^* = \theta - \omega_I t$ is the impeller-relative circumferential coordinate.

The pressure difference across the impeller due to the distorted flowfield is calculated by integrating Eq. (24). To facilitate this process, an impeller relative mean flow path and mean path velocity are defined such that

$$\boldsymbol{W}_m = V_r \boldsymbol{i}_r + W_\theta \boldsymbol{i}_\theta + V_z \boldsymbol{i}_z$$

$$\boldsymbol{i}_m = \cos\alpha_{1I}\boldsymbol{i}_r + \cos\alpha_{2I}\boldsymbol{i}_\theta + \cos\alpha_{3I}\boldsymbol{i}_z$$

With the assumption that the mean flow path is not altered by the unsteady perturbations, Eq. (24) is linearized and integrated along the mean path to give an expression for the unsteady pressure change across the impeller:

$$\left.\frac{\Delta p'}{\rho}\right|_{u,\mathrm{asy},I} = -\int_{s^*}\left(\frac{\bar{W}_\theta}{r}\frac{\partial W'_m}{\partial t} + \frac{\partial W'_m}{\partial t}\right)\mathrm{d}s^* \tag{25}$$

To transform this integral into a function of the perturbation waveforms at the inlet, mean and perturbation relative diffusion factors are defined, which relate the mean path velocity at the inlet with that at some point downstream:

$$\bar{W}_m(s^*) = \bar{D}_I \bar{W}_{mi}, \qquad \bar{W}'_m(s^*) = D'_I W'_{mi}$$

Substitution of these expressions into Eq. (25) gives

$$\left.\frac{\Delta p'}{\rho}\right|_{u,\mathrm{asy},I} = -W_m \left.\frac{\partial W'_m}{\partial \theta^*}\right|_i \int_{s^*}\frac{\cos\alpha_{2I}}{R}\bar{D}_I D'_I \,\mathrm{d}s^* - \left.\frac{\partial W'_m}{\partial t}\right|_i \times \int_{s^*} D'_I \,\mathrm{d}s^* \tag{26}$$

The derivatives of the mean flow perturbations at the inlet are related to the inlet axial flow:

$$\bar{W}_m \frac{\partial W'_m}{\partial \theta^*} = \bar{V}\frac{\partial V'_z}{\partial \theta^*} - U\frac{\partial V'_\theta}{\partial \theta^*} \tag{27}$$

$$\frac{\partial W'_m}{\partial t} = P\frac{\partial V'_z}{\partial t} - U\frac{\partial V'_\theta}{\partial t} \tag{28}$$

where

$$P \equiv \frac{\bar{V}}{\bar{W}_m} = \frac{\bar{\phi}}{\sqrt{\bar{\phi}^2 + 1}}, \qquad S \equiv \frac{U}{\bar{W}_m} = \frac{1}{\sqrt{\bar{\phi}^2 + 1}}$$

These expression are substituted into Eq. (26), along with the velocity relationships given by Eqs. (5), (9), and (10). The resulting equation, after transforming back to a fixed coordinate system, gives rise to the final expression for the unsteady, asymmetric pressure correction for the impeller:

$$\begin{aligned}\left.\frac{\Delta p'}{\bar{\rho}_i U^2}\right|_{u,\mathrm{asy},I} &= -\Gamma_{2I}\left[\frac{in}{f}\frac{\partial \phi'_p}{\partial \theta} + \frac{k}{\bar{\phi}n}\frac{\partial \phi'_v}{\partial \theta} + \bar{\phi}\frac{\partial \phi'}{\partial \theta}\right] \\ &\quad - \frac{R\Gamma_{1I}}{U}\left[P\frac{\partial \phi'}{\partial t} + S\left(\frac{in}{f}\frac{\partial \phi'_p}{\partial t} + \frac{k}{\bar{\phi}n}\frac{\partial \phi'_v}{\partial t}\right)\right] \\ &\quad - \Gamma_{1I}\left[P\frac{\partial \phi'}{\partial \theta} + S\left(\frac{in}{f}\frac{\partial \phi'_p}{\partial \theta} + \frac{k}{\bar{\phi}n}\frac{\partial \phi'_v}{\partial \theta}\right)\right]\end{aligned} \tag{29}$$

where

$$\Gamma_{1I} = \frac{1}{R}\int_{s^*}\frac{\bar{\rho}(s^*)}{\bar{\rho}_i} D'_I \,\mathrm{d}s$$

and

$$\Gamma_{2I} = \int_{s^*}\frac{\cos\alpha_{2I}}{r}\frac{\bar{\rho}(s^*)}{\bar{\rho}_i} D'_I \bar{D}_I \,\mathrm{d}s^*$$

Diffuser Correction

Proceeding in a similar manner for the diffuser, a mean velocity and flow path are defined in the stationary reference frame as

$$\boldsymbol{V}_m = V_r \boldsymbol{j}_r + V_\theta \boldsymbol{j}_\theta + V_z \boldsymbol{j}_z$$

$$\boldsymbol{j}_m = \cos\alpha_{1D}\boldsymbol{j}_r + \cos\alpha_{2D}\boldsymbol{j}_\theta + \cos\alpha_{3D}\boldsymbol{j}_z$$

Diffusion factors in the fixed reference frame are defined such that

$$\bar{V}_m(s^*) = \bar{D}_D \bar{V}_i, \qquad V'_m(s^*) = D'_D V'_{zi}$$

Thus, the pressure correction for the diffuser becomes

$$\left.\frac{\Delta p'}{\bar{\rho}_i U^2}\right|_{u,\mathrm{asy},D} = -\Gamma_{2D}\bar{\phi}\frac{\partial \phi'}{\partial \theta} - \frac{R\Gamma_{1D}}{U}\frac{\partial \phi'}{\partial t} \tag{30}$$

where

$$\Gamma_{1D} = \frac{1}{R}\int_{s^*}\frac{\bar{\rho}(s)}{\bar{\rho}_i} D'_D \,\mathrm{d}s$$

and

$$\Gamma_{2D} = \int_{s^*}\frac{\cos\alpha_{2D}}{r}\frac{\bar{\rho}(s)}{\bar{\rho}_i} D'_D \bar{D}_D \,\mathrm{d}s$$

Model for the Perturbation Diffusion Factors

The Γ parameters introduced in the preceding equation serve as weighting factors for the local and convective acceleration of the fluid in the impeller and diffuser. As expressed, they can be estimated from the steady diffusion and flow path of the fluid and the diffusion the unsteady perturbation experiences.

The perturbation diffusion factors D'_I and D'_D represent the change in the perturbation waveform as it passes through the compressor. For a potential disturbance in an incompressible flow, under the assumption of a constant mean flow path, the perturbation diffusion factors can be shown from continuity arguments to equal the steady values $\bar{D} = D'$. For a compressible flow, this relationship is no longer valid due to the influence of the density perturbation. In the absence of more detailed knowledge about the flow in the compressor, however, the assumption that the magnitude of the perturbation diffusion factor is equal to the steady value will be made. To account for finite propagation speeds for the disturbance, the perturbation diffusion factor is expressed as a complex quantity to account for a phase difference in the waveform between the inlet and a point in the flow path, taking the form

$$D' = \bar{D}e^{i\xi} \tag{31}$$

The phase lag will be a function of the wave propagation speed through the flow path. The simplest assumption would be that the vortical nature of the perturbation waveform is lost at the inlet of the compressor and the disturbance propagates at an infinite speed through an incompressible medium, and this was the assumption used for the earlier analysis of Ref. 9. If these assumptions are not made, two limiting cases present themselves. For a vorticity wave, the first is that the linear vortical nature of the velocity perturbation in the inlet is preserved and the wave convects with the mean flow velocity. For a potential disturbance, the second limiting case is that the wave propagates acoustically from the source of the disturbance.

To provide a quantitative expression of the preceding cases, the form of the phase lag for a simply convected vorticity wave, for the fixed reference frame, will be taken as

$$\xi_{vD} = -L_v \frac{\omega S_{vD}(s)}{\bar{V}(s)} \tag{32}$$

and, for the relative reference frame, as

$$\xi_{vI} = -L_v \frac{(\omega - n\omega_I) S_{vI}(s^*)}{\bar{W}(s^*)} \tag{33}$$

where S_v is the convection path length in the respective reference frame and L_v is a free parameter such that for $L_v = 1$ the wave is simply convected and for $L_v = 0$ the wave propagates at infinite speed.

In a similar manner the potential phase lags can be expressed for the fixed frame:

$$\xi_{pD} = -L_p \frac{\omega S_{pD}(s)}{\bar{a} \pm \bar{V}(s)} \tag{34}$$

and for the impeller relative frame:

$$\xi_{pI} = -L_p \frac{(\omega - n\omega_I) S_{pI}(s^*)}{\bar{a} \pm \bar{W}(s^*)} \tag{35}$$

where in this case the distance S_p refers to the distance from the source of the potential disturbance.

Neutral Stability Condition

The unsteady, asymmetric compressor characteristic comprises the terms described in Eqs. (19), (23), (29), and (30). For a given compressor geometry and steady flow performance specified by the characteristic and efficiency relationships, this unsteady characteristic takes the form

$$\psi' = \psi'(\bar{\phi}, k, \phi'_v, \phi')$$

This unsteady, asymmetric compressor characteristic is used to match the inlet total pressure perturbation described by Eq. (16) with the exit static pressure boundary condition of Eq. (17), resulting in

$$\psi' \equiv a_0 G_1 \phi' - G_2[(ik/f) + \bar{\phi}](\phi' - \phi'_v) \tag{36}$$

Equation (36) expresses the condition required for a neutrally stable potential wave to exist in the inlet. If it is assumed that the compressor, over a portion of the characteristic, had been capable of stable operation, then the point at which Eq. (36) is satisfied will mark the point of transition from negative to positive growth rates and, consequently, the stability boundary for a particular wave.

Control Effectiveness

For a simple control system, a corrective waveform of purely vortical nature is introduced into the compressor inlet at a phase and magnitude referenced to the total (potential plus vortical) disturbance waveform measured at the inlet. To facilitate this, a complex quantity Z is defined such that

$$Z = \phi'_v/\phi' = |Z|e^{i\beta}$$

This parameter is the complex control gain for a measured total perturbation at the inlet and vortical waveform controller response. It is useful to express the net perturbation in the inlet in terms of a complex amplitude A:

$$\phi' = Ae^{-in\theta}e^{i\omega t}, \qquad \phi'_v = ZAe^{-in\theta}e^{i\omega t}$$

$$\phi'_v = \phi' - \phi'_p = (A - ZA)Ae^{-in\theta}e^{i\omega t}$$

When these expressions are substituted into Eq. (36) and the exponential terms factored out, the final expression for the compressor stability boundary is obtained:

$$\begin{aligned} &a_0 G_1 \phi - G_2\left(\frac{ik}{f} + \bar{\phi}\right)(1 - Z) + \frac{\partial \bar{\psi}}{\partial \phi} \\ &\quad + \eta_c\left[\frac{in}{f}(1 - Z) + \frac{k}{\bar{\phi}n}Z\right]\left[1 + \frac{1}{\bar{p}_{ti}}\left(\bar{q}_e + \bar{\rho}_i U^2 \bar{\psi}\right)\right] \\ &\quad - \Gamma_{2I}\left[\frac{n^2}{f}(1 - Z) - \frac{ik}{\bar{\phi}}Z - in\bar{\phi}\right] \\ &\quad - \Gamma_{1I}\left[iPk - \frac{Snk}{f}(1 - Z) + \frac{ik^2}{\bar{\phi}n}Z - iPn\right. \\ &\quad \left. + \frac{Sn^2}{f}(1 - Z) - \frac{iSK}{\bar{\phi}}Z\right] + \Gamma_{2D} in\bar{\phi} - \Gamma_{1D} ik = 0 \end{aligned} \tag{37}$$

Equation (37) can be solved to determine the mean flow coefficient and reduced frequency of propagation at which a neutrally stable wave can exist in the inlet as a function of control magnitude and phase angle. The values of the flow coefficient thus determined can then be compared to that for the case where no control waveform is introduced to provide an indication of the effectiveness of the control.

Results and Discussion

The model represented by Eq. (37) was applied to the geometry of the Purdue Low-Speed Centrifugal Compressor (PLCC) facility described earlier. Recent experiments in this facility have focused on the detection of potential precursors to rotating stall and surge and, as such, provide a useful testbed for evaluating the mathematical model developed here.[6]

To apply the model to this compressor geometry, the steady, axisymmetric pressure characteristic and efficiency curves were estimated by fitting cubic polynomials to experimental prestall data obtained in the facility. The shapes of the curves beyond the stall point of the compressor are assumed to be a smooth extension of these curves. The four integral Γ parameters were calculated by numerical integration of diffusion factors and direction cosines estimated from flow areas and assumed flow paths through the impeller and diffuser sections.

Stall Initiation Prediction

The two cases that were selected for analysis with this mathematical model exhibit two distinctly different rotating stall pathologies, one resulting in a three-cell stall pattern and the other resulting in a

one-cell pattern. Both patterns are fast waves, traveling in excess of 75% of rotor speed. The pressure characteristics for the two cases are shown in Fig. 2.

The first configuration, case 1, consisted of 30 diffuser vanes with a stagger angle of 70 deg from the radial. In this configuration, the compressor enters a three-cell rotating stall pattern shortly after passing the peak of the pressure rise in the compressor. Results from the stall initiation experiments for this case are shown in Fig. 3. Figure 3 shows the magnitudes of the spatial Fourier transform from eight simultaneously sampled microphones in the o.d. endwall near the impeller inlet. The signals were numerically bandpass filtered to a 20-Hz band around the expected stall frequency, and then the spatial Fourier transform was performed. Analysis of these data showed that the waves presented in Fig. 3 are fundamental harmonics of independent modes rather than second or third harmonics of an impulsive stall cell. The arrows on the plots indicate the point at which the spatial waves are believed to enter a zone of amplification. The location of this point is based on the increase in magnitude of the given mode, as shown, and also an adjustment in phase propagation speed to that of the expected stall cell frequency. Note that the excitation of the first spatial mode in this plot is a one-per-revolution, machine-order pressure wave to the left of the indicated point. To the right of that point, the phase speed has changed to the final stall frequency of 24 Hz. Similar behavior is seen for the other modes. Detailed analyses of these data are presented in Ref. 6.

The predictions from the mathematical model for the stall point as compared to those determined experimentally are shown on an enlarged section of the pressure characteristic in Fig. 4. The model predicts the stall point somewhat earlier on the characteristic than the data indicate. It successfully predicts, however, that the higher modes arise first. In fact, the model predicts that modes higher than $n = 3$ will be amplified before that mode. Experimental data taken in the diffuser section of the compressor indicate that these higher modes, indeed, may be excited long before the main stall mode dominates the flowfield. The results shown from the mathematical model were obtained using Γ factors that were adjusted by decreasing the estimated diffusion factors in the impeller and diffuser sections by 4%. Initially, the third spatial mode became unstable at a flow coefficient $\phi = 0.31$, followed by the second and first modes. Reducing the diffusion factors slightly moved the stall point for the third mode to $\phi = 0.29$, as shown in Fig. 4. Although further numerical experimentation with the values of the Γ parameters was performed, the adjusted values did not produce results significantly better than the initial 4% correction to the diffusion factors.

The second compressor configuration investigated, case 2, utilized 15 diffuser vanes set, as in case 1, to a stagger angle of 70 deg from the radial. With the exception of adjusting the diffuser D value to reflect the increase in flow area, the same procedure was followed in calculating the Γ parameters as earlier employed. In this case, experimental results (Fig. 5) show an $n = 1$ rotating pattern arising first and eventually dominating the flowfield. An $n = 2$ pattern is observed to arise soon after the phase speed adjustment in the $n = 1$ pattern. No $n = 3$ pattern is observed in these experiments.

The predictions from the model for this case are especially encouraging. The model correctly predicts the $n = 1$ wave arising before the $n = 2$ wave. No zone of amplification is predicted for $n = 3$ or higher waves. The comparison between observed and predicted stall points is shown in Fig. 6.

For both case 1 and case 2, the phase speed of the pattern is underpredicted by the model. The wave speeds predicted for case 1 are on the order of 50% of rotor speed, and those for case 2 are on the order of 30% of rotor speed. This compares poorly with the observed propagation speeds in the PLCC facility of 80–90% of rotor speed. Nevertheless, the close spacing of the propagation speeds for the

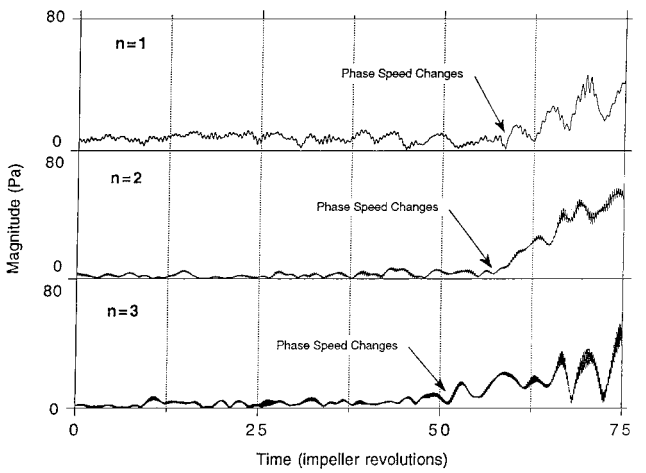

Fig. 3 Case 1, wave magnitudes for the first three spatial modes during stall.

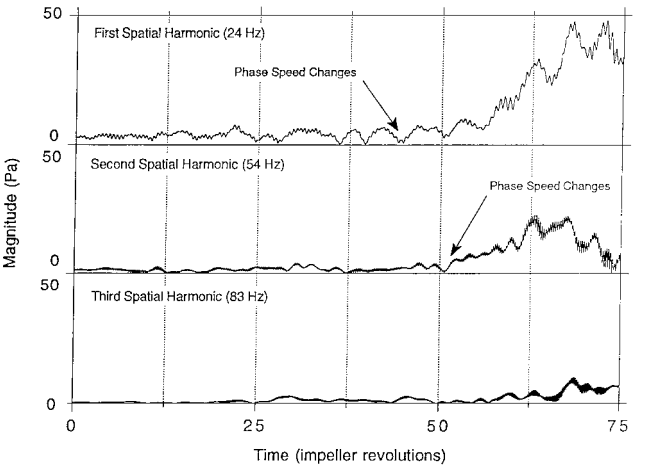

Fig. 5 Case 2, wave magnitudes for the first three spatial modes during stall.

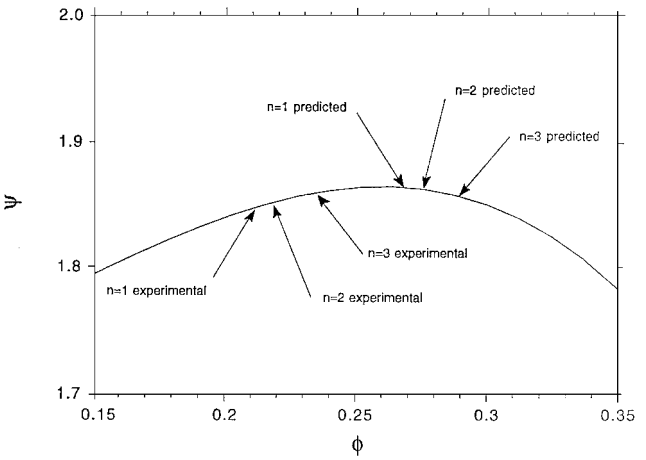

Fig. 4 Case 1, predicted and observed stall points.

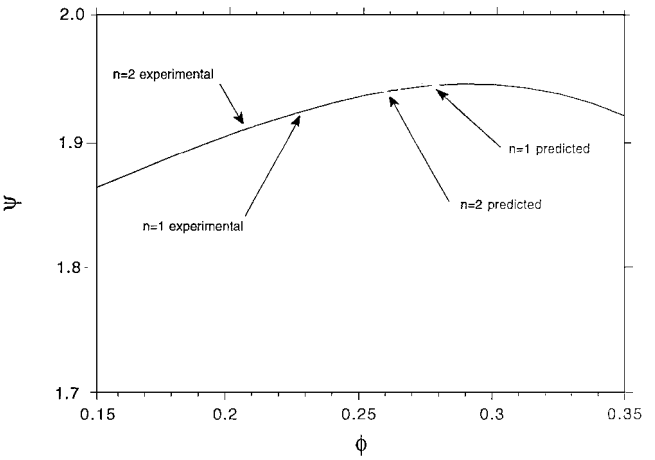

Fig. 6 Case 2, predicted and observed stall points.

various modes in a given configuration is reproduced by the model. Although full parametric studies have not been completed on the effect of the Γ parameters, it has been found that the wave speed is sensitive to the ratio of Γ_{1D} to Γ_{2D}.

The results for the prediction of the stalling point of the compressor provide assurance that the assumed parameters used in the model were of proper order of magnitude. These parameters were then used to investigate the effect that a control waveform would have on the amplification zones in the compressor operating range.

Control Effectiveness

With the introduction of the control vorticity wave in the inlet, the damping in the compression system changes and, therefore, the point on the characteristic at which a weak spatial pressure disturbance is amplified shifts. The following results present the change in the location of this stall point for a given spatial harmonic under the influence of the control waveform. The complex control gain magnitude and phase angle are plotted vs the percent change in the flow coefficient at neutral stability from the value when no control waveform is present. Positive values of $\Delta\bar{\phi}\%$ indicate a destabilization of the wave; negative values represent favorable stall suppression.

Results for the geometry of case 1 are shown in Figs. 7–9. In all of the cases, it is assumed that there is no potential phase lead or lag between the inlet and exit ($L_p = 0$). This assumption is consistent with a potential source near the vaneless space of the compressor.

Figures 7 and 8 present the effect of the control waveform if the vortical nature of the wave is preserved throughout the compressor flowpath ($L_v = 1$). Figure 7 shows the results for the $n = 3$ primary stall mode. Optimum phase angles for the control are centered around 225 deg. For control gain magnitudes greater than 6%, there is a rapid fall-off to stall suppressions greater that 50% of the original stall point. It is clear from this plot that the critical parameter for optimum effectiveness is the control phase angle. Destabilizing action from the control wave occurs if the phase angle is outside the optimum zone.

Figure 8 shows a similar plot for the $n = 2$ secondary mode for case 1. The control is less effective for a given wave magnitude than with the preceding $n = 3$ mode. The sharp transition to large stabilizing values is just beginning at a gain magnitude of 10%. The optimum control phase angle in this case is closer to 180 deg.

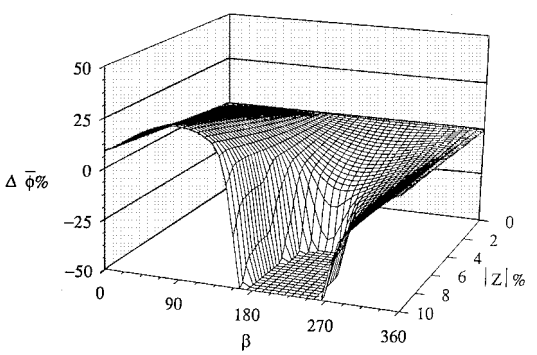

Fig. 7 Case 1, $n = 3$ wave and $L_v = 1$.

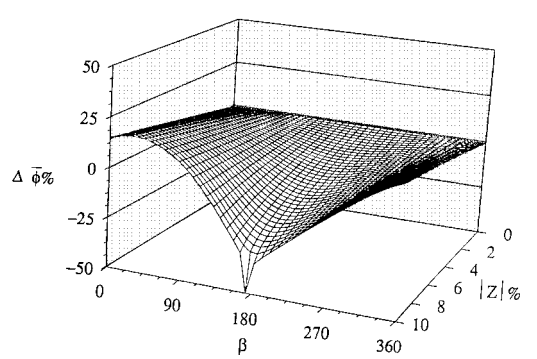

Fig. 8 Case 1, $n = 2$ wave and $L_v = 1$.

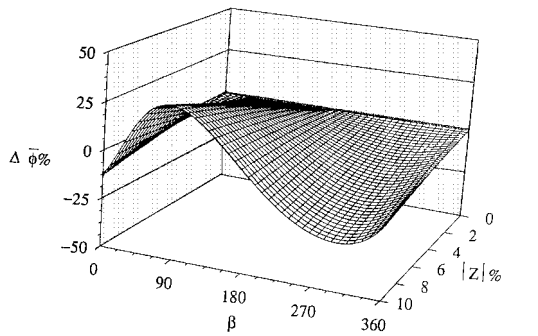

Fig. 9 Case 1, $n = 3$ wave and $L_v = 0$.

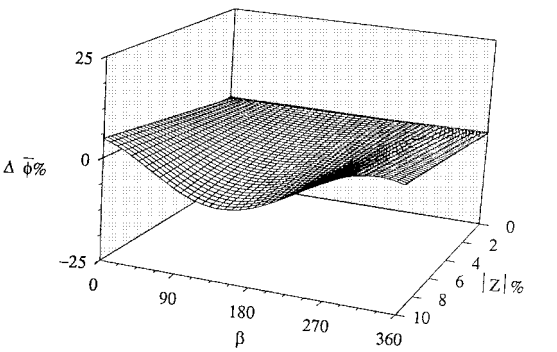

Fig. 10 Case 2, $n = 1$ wave and $L_v = 1$.

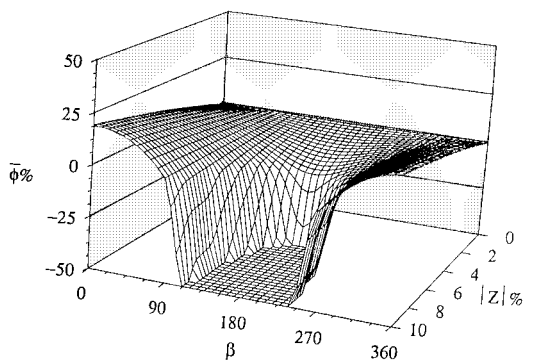

Fig. 11 Case 2, $n = 2$ wave and $L_v = 1$.

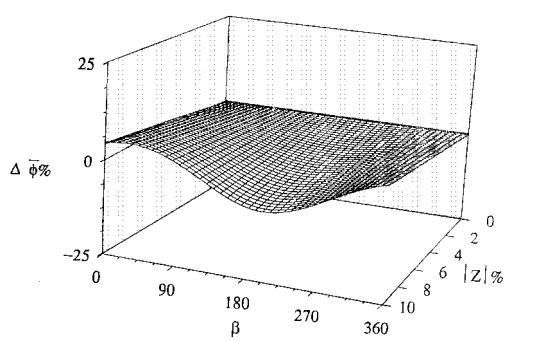

Fig. 12 Case 2, $n = 1$ wave and $L_v = 0$.

Figure 9 shows results for the $n = 3$ wave already considered in Fig. 7 with $L_v = 1$. In Fig. 9, however, the assumption is made that the vortical nature of the control waveform is lost at the inlet and the control waveform at the impeller face is in phase with that at the exit ($L_v = 0$). A comparison of Figs. 7 and 9 shows that the change in the lag parameter makes a profound difference in the results, with the control effectiveness substantially reduced and the optimum phase angle shifted to approximately 290 deg.

The results for case 2 are shown in Figs. 10–12. As with the earlier case, Figs. 10 and 11 assume a lag parameter of $L_v = 1$, and Fig. 10 shows the results for the primary $n = 1$ wave. This wave is significantly less responsive to the control waveform than the

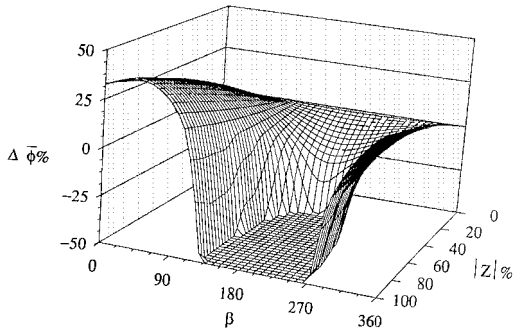

Fig. 13 Case 2, $n = 1$ wave and $L_v = 1$.

preceding cases, with a maximum control effectiveness of only −7% for the 10% gain magnitude level. The optimum phase angle for the control is near 150 deg.

Figure 11 shows the results for the secondary, $n = 2$ pattern. This case shows dramatically more response to the control, with suppressions greater than 50% for control wave magnitudes of only 5% of the total perturbation at the inlet. The optimum control phase is approximately 180 deg.

Figure 12 presents the results for the primary $n = 1$ mode if a lag parameter of zero is assumed ($L_v = 0$). Maximum control effectiveness decreased slightly to 6%, and the optimum control phase moved to 215 deg.

Figure 13 presents the same case as Fig. 11, the primary $n = 1$ mode with $L_v = 1$. In this plot, however, the control gain is extended to a value of 100%. This reveals that, although this mode is more resistant to the control waveform action, realistically obtainable control gains eventually achieve results similar to the others presented here.

Conclusions

The mathematical model developed by Lawless and Fleeter in Ref. 9 for the suppression of instabilities in a centrifugal compressor with a vaned diffuser has been extended to address the effects of finite waveform propagation speeds and subsonic compressibility effects. This model is based on the employment of control vortical waveform generated upstream of the impeller inlet to damp weak potential disturbances that are the early stages of rotating stall. The control system is analyzed by matching the perturbation pressure in the compressor inlet and exit flowfields with a model for the unsteady behavior of the compressor.

The model was effective at predicting the stalling behavior of the PLCC for two distinctly different stall patterns. Predictions made for the effect of a controlled inlet vorticity wave on the stability of the compressor show that for minimum control wave magnitudes, on the order of the total inlet disturbance magnitude, significant damping of the instability can be achieved. For control wave amplitudes of sufficient amplitude, the control phase angle appears to be the most important factor in maintaining a stable condition in the compressor.

The effect of introducing a lag to allow for the control wave to be convected through the compressor flow path in all cases was beneficial to the control effectiveness. The convected wave assumption also produced a shift in the phase angle for optimum control effectiveness.

Appendix: Relationship Between Perturbation Velocity and Perturbation Mach Number

Assume that the flow variables can be represented by time-averaged values and perturbation quantities such that

$$V = Ma \Rightarrow \bar{V} + V' = (\bar{M} + M')(\bar{a} + a') \tag{A1}$$

Ignoring terms of second order in the perturbation quantities gives

$$M' = (V'/\bar{a}) = \bar{M}(a'/\bar{a}) \tag{A2}$$

If the total temperature of the flow is constant, then

$$T_t = T + \frac{V^2}{2C_p} \Rightarrow \bar{T}_t = (\bar{T} + T') + \frac{\bar{V} + 2\bar{V}V'}{2C_p} + O(V'V')$$

$$T' = -\frac{\bar{V}V'}{C_p} \tag{A3}$$

For a perfect gas,

$$a^2 = \gamma RT \Rightarrow (\bar{a} + a')^2 = \gamma R(\bar{T} + T')$$

$$a' = (\gamma RT'/2\bar{a}) \tag{A4}$$

Using Eqs. (A2–A4), the required relationship is established:

$$M' = (V'/\bar{a})\{1 + [(\gamma - 1)/2]\bar{M}^2\} \tag{A5}$$

Or, in terms of mean flow coefficient and scaled acoustic speed,

$$M' = (V'/\bar{a})\left\{1 + [(\gamma - 1)/2](\bar{\phi}/a_0)^2\right\} \tag{A6}$$

Acknowledgments

This research was sponsored in part by the Army Aviation Systems Command, NASA Lewis Research Center, and the Army Research Office. This support is most gratefully acknowledged.

References

[1] Day, I. J., "Active Suppression of Stall and Surge in Axial Compressors," *Journal of Turbomachinery*, Vol. 115, Jan. 1993, pp. 40–47.

[2] McDougall, N. M., Cumpsty, N. A., and Hynes, T. P., "Stall Inception in Axial Compressors," *Journal of Turbomachinery*, Vol. 112, Jan. 1990, pp. 116–125.

[3] Garnier, V. H., Epstein, A. H., and Greitzer, E. M., "Rotating Stall Anticipation and Initiation in Axial Compressors," American Society of Mechanical Engineers, ASME Paper 90-GT-156, June 1990.

[4] Frigne, P., and Van Den Braembussche, R., "Distinction Between Different Types of Impeller and Diffuser Rotating Stall in a Centrifugal Compressor with Vaneless Diffuser," *Journal of Engineering for Gas Turbines and Power*, Vol. 106, April 1984, pp. 468–474.

[5] Moore, F. K., "Weak Rotating Flow Disturbances in a Centrifugal Compressor with a Vaneless Diffuser," *Journal of Turbomachinery*, Vol. 111, Oct. 1989, pp. 442–449.

[6] Lawless, P. B., and Fleeter, S., "Rotating Stall Acoustic Signature in a Low Speed Centrifugal Compressor Part II: Vaned Diffuser," American Society of Mechanical Engineers, ASME Paper 93-GT-254, May 1993.

[7] Epstein, A. H., Ffowes Williams, J. E., and Greitzer, E. M., "Active Suppression of Aerodynamic Instabilities in Turbomachines," *Journal of Propulsion and Power*, Vol. 5, No. 2, 1989, pp. 204–211.

[8] Paduano, J., Epstein, A. H., Valavani, L., Longley, J. P., Greitzer, E. M., and Guenette, G. R., "Active Control of Rotating Stall in a Low Speed Axial Compressor," *Journal of Turbomachinery*, Vol. 115, Jan. 1983, pp. 48–56.

[9] Lawless, P. B., and Fleeter, S., "Active Unsteady Aerodynamic Suppression of Rotating Stall in an Incompressible Flow Centrifugal Compressor with Vaned Diffuser," AIAA Paper 91-1898, June 1991.

[10] Goldstein, M. E., "Unsteady Vortical and Entropic Distortions of Potential Flows Round Arbitrary Obstacles," *Journal of Fluid Mechanics*, Vol. 89, No. 3, 1978, pp. 433–468.

S. Glegg
Associate Editor